Effects of nozzle-lip thickness on the tones in the near-field pressure spectra of high-speed jets

Christophe Bogey*

Univ Lyon, CNRS, Ecole Centrale de Lyon, INSA Lyon, Univ Claude Bernard Lyon I,
Laboratoire de Mécanique des Fluides et d'Acoustique, UMR 5509, 69130 Ecully, France

The effects of the nozzle-lip thickness on the near-field pressure spectra of free jets are investigated by computing initially laminar isothermal jets at Mach numbers $M = 0.6$, 0.9 and 1.3 for lip thicknesses equal to 0.014, 0.058, 0.023 and 0.093 times the nozzle radius. For a thicker lip, the jet mixing layers develop more rapidly and contain stronger low-frequency components, notably near the cut-off frequencies of the first radial modes of the free-stream upstream-propagating guided jet waves (GJW). More prominent or additional peaks are also generally found in the pressure spectra outside the mixing layers at the frequencies mentioned above. The variations of the peak properties as the nozzle-lip thickness increases depend on the Mach number and the location where the spectra are calculated. Inside the potential core, the tones in the spectra for $M = 0.9$ do not change appreciably, whereas narrow peaks emerge by 3 dB for $M = 0.6$ and 1.3, including one near the frequency of the least-dispersed waves of the first axisymmetric GJW mode in the subsonic case. Outside the jet, near the nozzle, the levels of the tones obtained for $M = 0.9$ and 1.3 grow by at most 3 dB and 6 dB, while the broadband peaks appearing in the spectra for $M = 0.6$ turn into 2 dB stronger, narrower peaks. Therefore, with one exception, a thicker nozzle lip promotes the establishment of tonal components in the pressure spectra of the jets, most likely by enhancing the reflection of the free-stream GJW at the lip. The exception, concerning the tones in the jet for $M = 0.9$, can be explained by the fact that the upstream-propagating waves responsible for the latter are duct-like GJW.

I. Introduction

For screeching and impinging jets in which aeroacoustic feedback loops establish and generate tones in the acoustic field, the scattering of upstream-propagating waves into Kelvin-Helmholtz instability waves at the nozzle-exit section via a receptivity process is a key element for closing the loops, as pointed out in the reviews by Raman [1] and Edgington-Mitchell [2]. The efficiency of the receptivity process has been investigated by many researchers, qualitatively but also quantitatively as in Karami et al. [3] and Mancinelli et al. [4], for instance. It was shown to depend on several flow parameters, such as the angle of incidence, the azimuthal mode number and the frequency of the waves hitting the nozzle, but also on geometric parameters. Thus, for impinging jets, the strengths of the feedback loops are sensitive to the external geometry of the nozzle and to the presence of reflective surfaces upstream of the jets, as illustrated in Weightman et al. [5] and Karami and Soria [6]. For screeching jets, they have been known to be sensitive to the thickness of the nozzle lip, on which upstream-propagating waves are reflected back and force the near-nozzle shear layer, at least since the work of Powell [7]. The inclusion of a thicker lip usually results in stronger screech tones, whereas very thin lips may lead to screech cessation, as reported in the papers by Norum [8], Ponton and Seiner [9], Raman [10] and Shen and Tam [11], among others.

For subsonic and non-screeching supersonic free jets, the influence of the nozzle lip has been the subject of very few investigations, because of the long shared belief that the receptivity process plays a negligible role in these jets. In support of this, the nozzle-lip thickness was found to have no effect on the noise levels and spectra and on the near-nozzle turbulence of subsonic jets in the experiments of Olsen et al. [12] and Fontaine et al. [13]. Olsen et al. [12] noted, however, that a screech component can occur at subsonic velocities when a large flat plate is placed at the nozzle orifice and concluded that this type of nozzle shape should be avoided in jet noise experiments. In Zaman [14, 15], significant differences in subsonic jet noise levels were also observed using two rectangular nozzles with identical internal geometries, the first one with a thin lip and the second one with a perpendicular face at the exit. They were attributed to changes in the boundary-layer state, the nozzle-exit boundary layer being laminar in the first case but turbulent in the second one, and not to an alteration of the receptivity process at the nozzle lip.

Although the possibility was proposed by Laufer and Monkewitz [16] and Ho and Huang [17] forty years ago, it has been also widely admitted for a very long time that feedback loops do not exist in free jets containing no shocks. This idea was, however, questioned by the measurements made by Suzuki and Colonius [18] in 2006 revealing the emergence of tones in the near acoustic fields of high subsonic jets. A decade later, the presence, physical origin and properties of these tones were investigated in a series of theoretical, experimental and numerical studies by Towne et al. [19], Schmidt et al. [20], Brès et al. [21], Zaman et al. [22] and Bogey [23, 24], among others. These authors demonstrated that the waves essentially confined in the jets first described by Tam and Hu [25], sometimes called neutral acoustic waves and referred to as guided jet waves (GJW) in what follows, can lead to the generation of acoustic tones in the jet potential core, in the acoustic field near the nozzle and in the far field in the upstream direction. The GJW are characterized by specific dispersion relations depending on the Mach number and they are of duct-like nature when their amplitude is zero on the nozzle lip-line and outside the jet and of free-stream nature otherwise. In a recent work [26], the free-stream upstream-propagating GJW were shown to force the Kelvin-Helmholtz instability waves growing in the shear layers of free jets with laminar boundary layers. We can wonder whether the nozzle-lip thickness affects the efficiency of this coupling and, consequently, the resulting components in the pressure spectra inside and outside the jet flow.

In the present study, on the basis of the above, the influence of the nozzle-lip thickness on the tones possibly appearing in the near-field pressure spectra of subsonic and non-screeching supersonic free jets is investigated. For that purpose, initially laminar isothermal jets at Mach numbers $M = 0.6$, 0.9 and 1.3 and a Reynolds number of 10^5, exhausting from pipe nozzles with lips of four different thicknesses, are computed using large-eddy simulations (LES). The Mach numbers are chosen to cover the three types of results expected in the pressure spectra of subsonic Mach numbers below and above $M = 0.8$ and of supersonic Mach numbers [19, 23], namely the presence of tones inside the potential core for $M = 0.9$ but not for $M = 0.6$ and 1.3 and of broadband and tonal components outside the flow near the nozzle exit for $M = 0.6$ and for $M = 0.9$ and 1.3, respectively. The nozzle-lip thicknesses range between 0.014 and 0.93 times the nozzle radius to consider both very thin and very thick lips. The objective will be to determine whether the use of a thicker lip results in stronger or additional tones in the pressure fields inside and outside of the jets, as in screeching jets, and to changes in the tone frequencies. For that, the amplitudes, widths and frequencies the peaks that will be detected in the pressure spectra calculated in the jet potential core and near the nozzle will be presented. The peak frequencies will also be compared with those predicted for the free-stream upstream-propagating GJW using a vortex-sheet model. Thus, based on the variations of the peak amplitudes with the nozzle-lip thickness and on the peak frequencies, it will be possible to discuss whether the peaks are linked to upstream-propagating GJW and, if so, to identify the nature of the latter (free-stream, duct-like, least-dispersed GJW for example).

The paper is organized as follows. In section II, the jet initial conditions and the LES methods and parameters are presented. In section III, vorticity and pressure snapshots are first displayed. Then, the main characteristics of the velocity fields obtained in the jet mixing layers, and pressure spectra calculated inside and outside the jet flow are shown. The presence of peaks and tonal components in the spectra and the variations of their properties with the nozzle-lip thickness are discussed. Finally, concluding remarks are given in section IV.

II. Parameters

A. Jet flow conditions

Twelve isothermal round free jets at a Reynolds number $\text{Re}_D = u_j D / \nu = 10^5$, four at a Mach number $M = u_j / c_0 = 0.6$, four at $M = 0.9$ and four at $M = 1.3$, where u_j, c_0, D and ν are the jet velocity, the speed of sound in the ambient medium, the nozzle diameter and the kinematic molecular viscosity, are considered. They originate from a pipe nozzle of radius $r_0 = D/2$ and length $2r_0$ into a medium at ambient temperature and pressure $T_0 = 293$ K and $p_0 = 10^5$ Pa. At the pipe inlet, at $z = -2r_0$, a Blasius laminar boundary-layer profile of thickness $\delta_{BL} = 0.1r_0$ is imposed for the axial velocity [27]. Radial and azimuthal velocities are set to zero, pressure is equal to p_0 and temperature is determined by a Crocco-Busemann relation. The exit of the pipe nozzle is at $z = 0$ and its thickness δ_{lip} varies geometrically from $\delta_{lip} \simeq 0.01r_0$ up to $\delta_{lip} \simeq 0.9r_0$. More precisely, for the four jets at a given Mach number, the nozzle-lip thickness is equal to $\delta lip(0)/4 = 0.014r_0$, $\delta lip(0) = 0.058r_0$, $4\delta lip(0) = 0.23r_0$ and $16\delta lip(0) = 0.93r_0$, where $\delta lip(0)$ is the value specified in several former jet LES of the author [23, 26–31]. In what follows, the nozzle-lip thicknesses will be referred to as dlipx1, dlipx4, dlipx16 and dlipx64, from the smallest to the largest.

In order to shorten the simulation transitory period, pressure fluctuations of maximum amplitude 200 Pa random in both space and time are introduced outside the nozzle in the shear layers between $z = 0.25r_0$ and $z = 4r_0$ from time

$t = 0$ up to $t = 12.5r_0/u_j$. Afterwards, the jet turbulent development is not sustained by any artificial forcing. Indeed, the boundary layers inside the nozzle are untripped. As a consequence, the nozzle-exit mean velocity profiles do not deviate appreciably from the the pipe-inlet profile and are superimposed on each other as illustrated in figure 1. They are characterized by a momentum thickness of $\delta_\theta \simeq 0.012r_0$. For the comparison, this value is twice as large as that of $\delta_\theta = 0.006r_0$ measured by Zaman [32] in an untripped jet at $\mathrm{Re}_D = 10^5$. The root-mean-square (r.m.s.) values of axial velocity fluctuations are represented in figure 2. Their peak values u'_e at the nozzle exit do not exceed 0.5 per cent of u_j, indicating that the jets are all initially fully laminar. The r.m.s. levels of velocity fluctuations can be noted to increase with the nozzle-lip thickness, weakly for M = 0.6 but more significantly for the two other Mach numbers. Thus, the peak values of u'_e/u_j rise only from 0.14% up to 0.18% for M = 0.6, but from 0.23% up to 0.42% for M = 0.9 and from 0.23% up to 0.48% for M = 1.3. These results suggest the presence of stronger waves propagating upstream along the nozzle-lip line for a thicker lip, which will be later discussed.
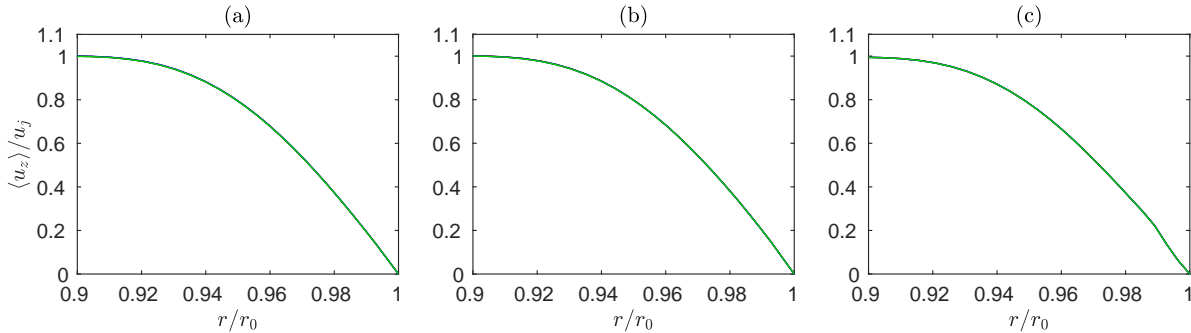
Fig. 1   Nozzle-exit profiles of the mean axial velocity for (a) $M = 0.6$, (b) $M = 0.9$ and (c) $M = 1.3$: ——— dlipx1, ——— dlipx4, ——— dlipx16 and ——— dlipx64.
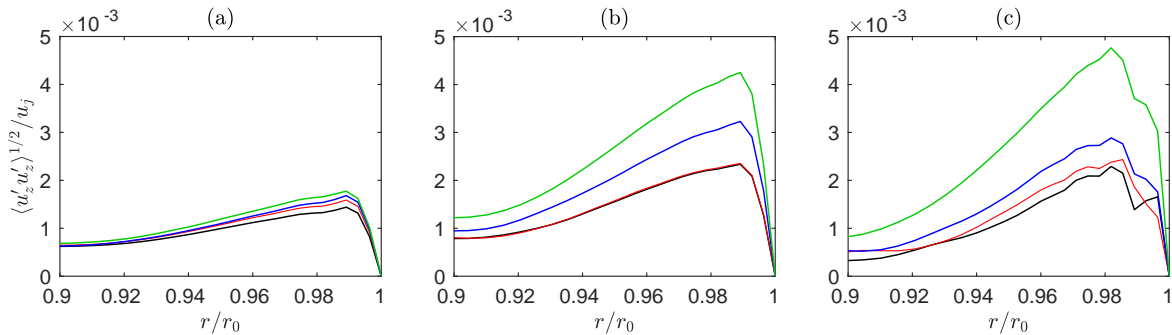
Fig. 2   Nozzle-exit profiles of the r.m.s. values of axial velocity fluctuations for (a) $M = 0.6$, (b) $M = 0.9$ and (c) $M = 1.3$: ——— dlipx1, ——— dlipx4, ——— dlipx16 and ——— dlipx64.

B. Numerical methods

The jets are computed using the same framework as in previous jet simulations of the author [23, 26–31]. The LES are carried out by solving the three-dimensional compressible Navier-Stokes equations in cylindrical coordinates (r, θ, z) using low-dissipation and low-dispersion explicit schemes. The axis singularity is taken into account by the method of Mohseni and Colonius [33]. In order to alleviate the time-step restriction near the cylindrical origin, the derivatives in the azimuthal direction around the axis are calculated at coarser resolutions than permitted by the grid [34]. For the points closest to the jet axis, they are evaluated using 16 points, yielding an effective resolution of $2\pi/16$. Fourth-order eleven-point centered finite differences are used for spatial discretization, and a second-order six-stage Runge-Kutta algorithm is implemented for time integration [35]. A sixth-order eleven-point centered filter [36] is applied explicitly to the flow variables every time step. Non-centered finite differences and filters are also used near the pipe walls and the grid boundaries [27, 37]. For the jets at M = 1.3 containing weak shock cells in their potential cores, a shock-capturing filtering is applied in order to avoid Gibbs oscillations near the shocks. It consists in applying a conservative second-order filter at a magnitude determined each time step using a shock sensor [36]. At the boundaries,

3

the radiation conditions of Tam and Dong [38] are applied, with the addition at the outflow of a sponge zone combining grid stretching and Laplacian filtering in order to avoid significant acoustic reflections. Small adjustment terms are also added to prevent that mean density and pressure deviate significantly from ambient density and pressure, and no co-flow is imposed. In the present simulations, the explicit filtering is employed to remove grid-to-grid oscillations, but also, as the mesh grid is not fine enough to compute the smallest turbulent structures, as a subgrid-scale high-order dissipation model in order to relax turbulent energy from scales at wave numbers close to the grid cut-off wave number while leaving larger scales mostly unaffected. The performance of this large-eddy simulation (LES) approach has been assessed in past studies for subsonic jets, Taylor-Green vortices and turbulent channel flows [39–41].

C. Simulation parameters

The same grid is used in the (r, z) section in all simulations. It was constructed in a grid-sensitivity study [30] carried out for three jets at M = 0.9, two with untripped boundary layers with $\delta_{BL} = 0.2r_0$ and $0.025r_0$ and one with tripped boundary layers with $\delta_{BL} = 0.15r_0$. The grid contains $N_r = 512$ points in the radial direction and $N_z = 2,085$ points in the axial direction. Its physical extents are $L_r = 15r_0$ and $L_z = 40r_0$. The minimum radial and axial mesh spacings are found near the nozzle lip and are equal to $\Delta r = 0.0036r_0$ between $r = r_0$ and $r = r_0 + \delta_{lip}$ and to $\Delta z = 0.0072r_0$ at $z = 0$. The maximal mesh spacing is equal to $\Delta r = 0.075r_0$ in the jet near field, leading to the Strouhal number of $St_D = fD/u_j = 8.9$ for M = 0.6, 5.9 for M = 0.9 and 4.1 for M = 1.3 for an acoustic wave discretized by five points per wavelength, where f is the frequency. In the azimuthal direction, there are $N_\theta = 512$ points for the jet at M = 0.9 with dlipx4, simulated in recent work [23, 26], and $N_\theta = 256$ points in the other cases. Approximately 100 GB and 50 GB of memory are required, respectively.

The simulations have been performed with an OpenMP-based in-house solver using a time step Δt of $0.7 \times \min(\Delta r)/c_0$ in order to ensure numerical stability in all cases. The simulation time T after the transient period is equal to $2,000r_0/u_j$ for the jets at M = 0.6 and to $1,500r_0/u_j$ for M = 0.9 and 1.3. It is longer in the first case where spectra are broadband than in the second ones where tonal components strongly emerge [23]. During time T, density, velocity components and pressure have been recorded at several locations, see in reference [42] for an exhaustive description of the data available. The data of interest in this work include those on the jet centerline at $r = 0$, on the nozzle lip-line cylindrical surface at $r = r_0$ and on the nozzle-exit cross section at $z = 0$, which have been stored at a sampling frequency corresponding to $St_D = 12.8$. The signals have also been acquired in the azimuthal planes at $\theta = 0$, $\pi/4$, $\pi/2$ and $3\pi/4$ at a sampling frequency of $St_D = 6.4$. The Fourier coefficients estimated over the section (r, z) have been saved in the same way for the azimuthal modes $n_\theta = 0$ to 8 for the jets computed using the nozzle-lip thickness dlipx4 and from $n_\theta = 0$ to 4 otherwise. The statistics are averaged in the azimuthal direction, when possible. The time spectra are evaluated from overlapping samples of duration $45r_0/u_j$ on the jet axis, and $90r_0/u_j$ otherwise.

III. Results

A. Vorticity and pressure snapshots

Fields of the vorticity norm and of the pressure fluctuations $p - p_0$ obtained in the (z, r) plane near the nozzle between $z = -0.5r_0$ and $z = 5.5r_0$ are represented in figures 3(left) for the jets at $M = 0.6$, in figures 3(middle) for $M = 0.9$ and in figures 3(right) for $M = 1.3$ for the four nozzle-lip thicknesses. The pipe-nozzle lips, displayed in black, thicken from top to bottom.

In the vorticity fields, in all cases, Kelvin-Helmholtz instability waves, whose footprints can be seen in the pressure fields, initially grow in the laminar mixing layers. As expected [43], they lead to the shear-layer rolling-up, then to a first stage of pairings of vortical coherent structures and finally to 3-D turbulent fields. The shear-layer rolling-up occurs later as the Mach number increases, due to the lower amplification rates of the instability waves [44, 45]. For a given Mach number, it seems to happen slightly farther upstream for a thicker nozzle lip. Apart from that, the jet flow does not change much.

In the pressure fields, in addition to the low-frequency hydrodynamic disturbances associated with the instability waves and the shear-layer large-scale structures [46], acoustic waves appear on both sides of the mixing layers. Weak shock cells are also visible in the jets at $M = 1.3$, despite the fact that ambient pressure is imposed at the inlet of the pipe nozzle. Regarding the acoustic waves inside and outside the jet potential core, they are particularly strong for $M = 0.9$ and $M = 1.3$. Outside the jet, for the two latter Mach numbers, they may be more intense for dlipx16 in figures 3(k,l) than for thinner nozzle lips.

4
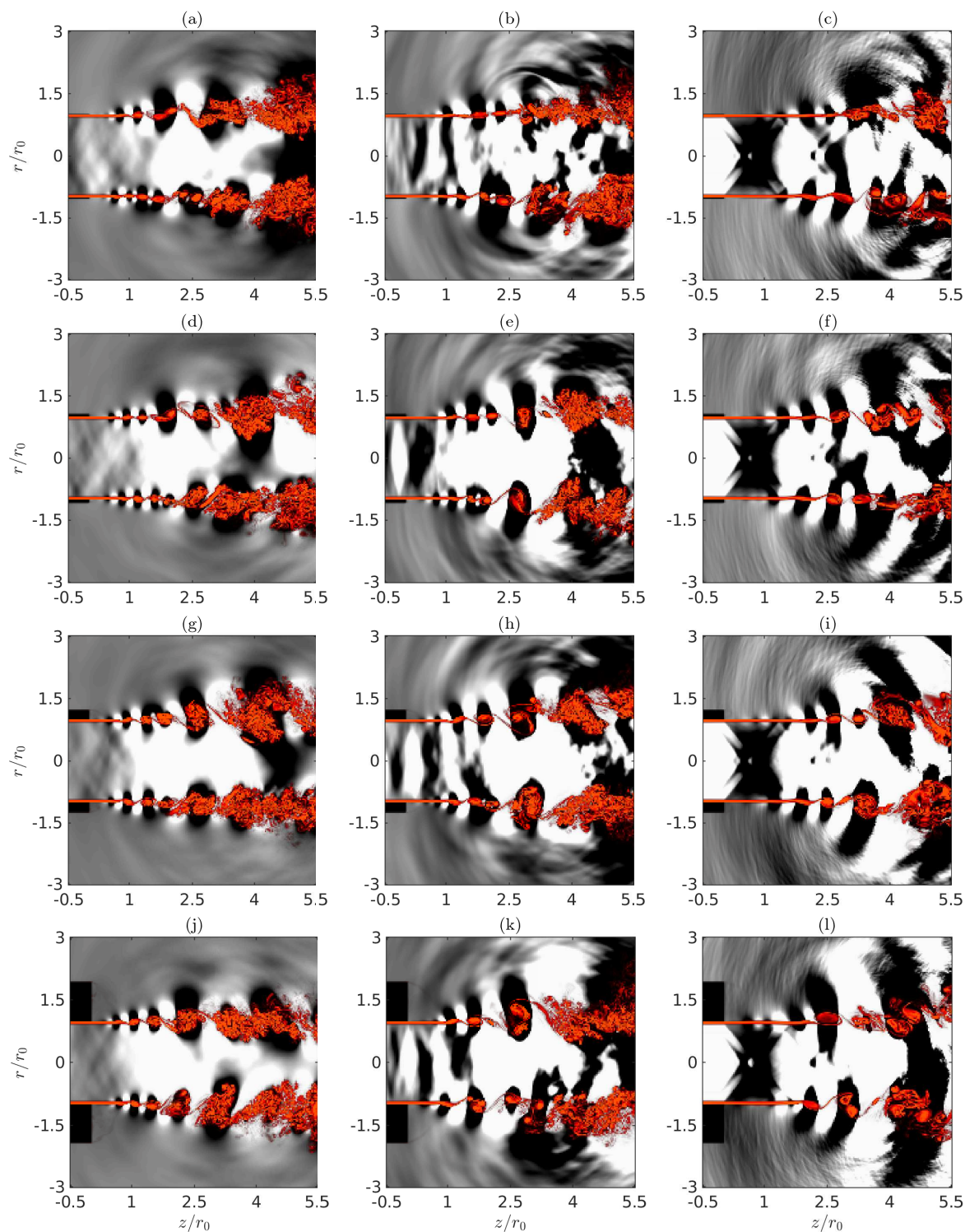
Fig. 3 Snapshots of vorticity norm and pressure fluctuations for (left) $M = 0.6$, (middle) $M = 0.9$ and (right) $M = 1.3$: (a-c) dlipx1, (d-f) dlipx4, (g-i) dlipx16 and (j-l) dlipx64. For vorticity, the color scale levels range from 0 to $12u_j/r_0$, from white to red; for pressure, the grey scale levels range between (left) $\pm 3.5 \times 10^{-3} p_0$, (middle) $\pm 4.75 \times 10^{-3} p_0$ and (right) $\pm 7.5 \times 10^{-3} p_0$.

5

B. Jet flow development

The influence of the nozzle-lip thickness on the jet flow field is first briefly examined. For a thicker lip, indeed, the jet development may be affected by a stronger forcing of the shear layer by the upstream-propagating waves or by a change in the entrainment process of the ambient medium near the nozzle.

To describe the properties of the shear-layer fluctuations just downstream of the nozzle, the spectra of the radial velocity fluctuations at $r = r_0$ and $z = 0.4r_0$ are represented in figure 4 as a function of St_D. The most unstable frequencies calculated for the mode $n_\theta = 0$ from the LES mean flow fields at $z = 0.2r_0$ by a linear stability analysis [44] using the same procedure as in previous work [26, 31, 47] are indicated. The cut-off Strouhal numbers of the first radial modes of the free-stream upstream-propagating GJW obtained for $n_\theta = 0$, 1 and 2 using a vortex-sheet model [25] are also depicted. As defined in reference [23], they correspond, for $M = 0.6$, to the frequencies of the least-dispersed GJW [48] at the inflection points I on their dispersion curves. For $M = 0.9$ and 1.3, they are found at the stationary points S_{max} (saddle points S2 in Towne et al. [19]), or at the limit points L on the line $k = -\omega/c_0$ when the points S_{max} do not exist, where k and ω are the wavenumber and the pulsation.

For all jets, a large hump is observed around the most unstable frequencies around $St_D = 2$, as expected. Strong components also appear at lower frequencies, including peaks at specific Strouhal numbers, for instance at $St_D = 1$ for $M = 0.6$ in figure 4(a) and at $St_D = 0.4$ and 0.7 for $M = 0.9$ in figure 4(b). The peak Strouhal numbers do not vary much with the nozzle-lip thickness and agree well with the cut-off frequencies of the free-stream GJW. Therefore, the peaks result from the forcing of the shear-layer instability waves by the latter waves, as was documented recently [26]. Moreover, as the nozzle lip is thicker, the levels rise at all frequencies. This trend is consistent with the increase of the nozzle-exit turbulence intensities in figure 2, which is most likely due to more intense upstream-propagating waves. The rise of the levels, however, is higher in the shear layer than at the nozzle exit, suggesting also a greater efficiency of the receptivity process near the lip as the nozzle-exit reflective surface is larger.
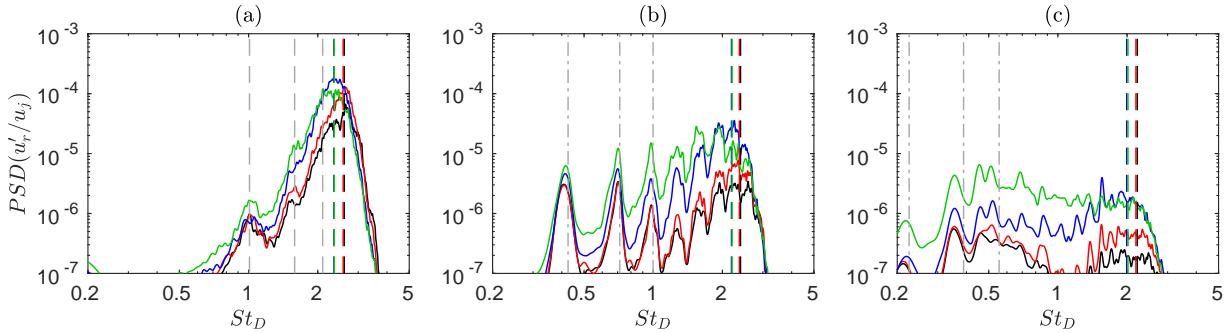
Fig. 4   Power spectral densities of radial velocity fluctuations at $r = r_0$ at $z = 0.4r_0$ for (a) $M = 0.6$, (b) $M = 0.9$ and (c) $M = 1.3$: —— dlipx1, —— dlipx4, —— dlipx16 and —— dlipx64; cut-off Strouhal numbers of the first radial modes $n_\theta = 0$, 1 and 2 of the free-stream upstream-propagating GJW at points — — — I and — · — S_{max} or L on the GJW dispersion curves for a vortex sheet; (other dashed lines) most unstable frequencies at $z = 0.2r_0$ for $n_\theta = 0$ using the same colors as for the solid lines.

To characterize the laminar-turbulent transition in the jet mixing layers, the r.m.s. values of the radial velocity fluctuations obtained at $r = r_0$ are represented in figure 5 between $z = 0$ and $z = 10r_0$. In all cases, as classically observed for initially laminar flow conditions [49, 50], the levels rapidly grow and reach peak values approximately of 20 per cent of u_j, The profiles exhibit dual-peak shapes, which are due to a first stage of vortex pairings happening at a fixed location [27, 51]. As the nozzle-lip thickness increases, the fluctuation levels start to rise slightly earlier, which is not surprising given the velocity spectra of figure 4. As a result, the peak values are achieved farther upstream and, the positions $z_{turb10\%}$, where the r.m.s. value of the radial velocity fluctuations is equal to $0.10u_j$, for instance, vary from $z_{turb10\%} = 0.90r_0$ to $0.77r_0$ for $M = 0.6$ in figure 5(a), from $z_{turb10\%} = 1.28r_0$ to $1.04r_0$ for $M = 0.9$ in figure 5(b) and from $z_{turb10\%} = 2.37r_0$ to $1.92r_0$ for $M = 1.3$ in figure 5(c).

Finally, the variations of the centerline mean axial velocity between $z = 0$ and $z = 18r_0$ are represented in figure 6. Oscillations due to the presence of weak shock cells can be noted in the potential core of the jets at $M = 1.3$ in figure 6(c). Overall, the velocity profiles do not change dramatically with the nozzle-lip thickness. As the latter increases, however, the jet potential core is slightly longer for $M = 0.6$ but is shorter for the two other Mach numbers, especially for dlipx64. Thus, the location z_c of the end of the potential core, where, arbitrarily, $\langle u_z \rangle (z_c) = 0.9u_j$,
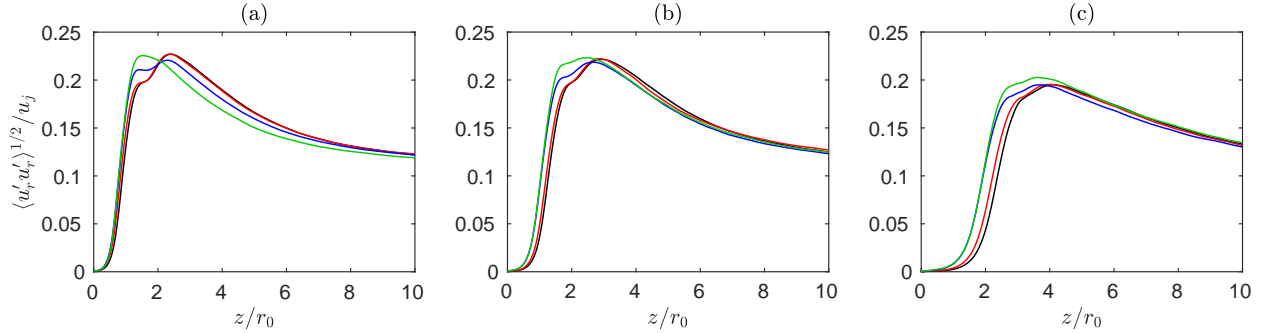
Fig. 5 **Variations of the r.m.s. values of radial velocity fluctuations at $r = r_0$ for (a) $M = 0.6$, (b) $M = 0.9$ and (c) $M = 1.3$:** ——— **dlipx1,** ——— **dlipx4,** ——— **dlipx16 and** ——— **dlipx64.**

varies from $z_c = 10.7r_0$ to $11.3r_0$ for $M = 0.6$ in figure 6(a), from $z_c = 10.7r_0$ to $10.4r_0$ for $M = 0.9$ in figure 6(b) and from $z_c = 11.5r_0$ to $10r_0$ for $M = 1.3$ in figure 6(c).
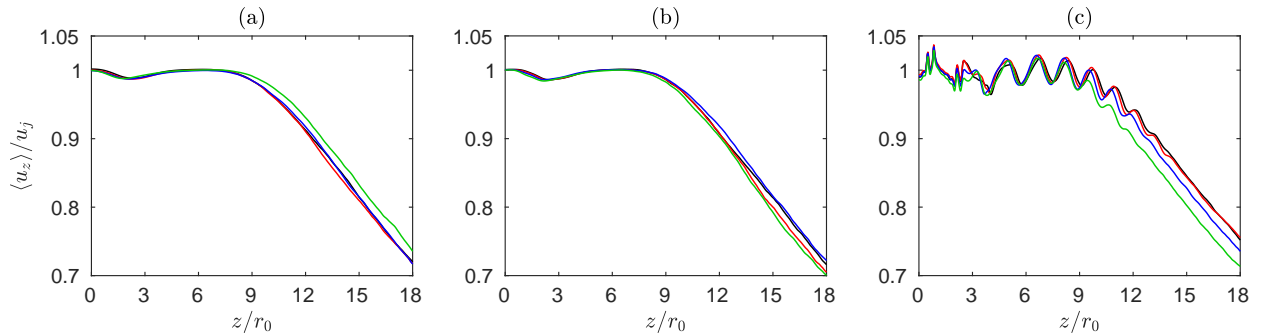
Fig. 6 **Variations of the mean axial velocity at $r = 0$ for (a) $M = 0.6$, (b) $M = 0.9$ and (c) $M = 1.3$:** ——— **dlipx1,** ——— **dlipx4,** ——— **dlipx16 and** ——— **dlipx64.**

C. Pressure spectra in the jet potential core

The existence of tonal components in the jet potential core as the nozzle-lip thickness varies is now examined. For that, spectra of pressure fluctuations have been calculated at $r = 0$ for the azimuthal mode $n_\theta = 0$, at $r = 0.2r_0$ for $n_\theta = 1$ and at $r = 0.3r_0$ for $n_\theta = 2$. Because of the possible presence at the tonal frequencies of standing wave patterns, hence of nodes and antinodes, they have been averaged between $z = 0$ and $z = z_c/2$. The results obtained for $n_\theta = 0$ and $n_\theta = 1$ are represented as a function of St_D in figures 9(left) for the jets at $M = 0.6$, in figures 9(middle) for $M = 0.9$ and in figures 9(right) for $M = 1.3$. The results for $n_\theta = 2$, not shown for brevity, exhibit the same trends as those for $n_\theta = 1$. The cut-off Strouhal numbers of the first radial modes of the free-stream upstream-propagating GJW are also displayed. As reported in previous section, they correspond to the frequencies at the points I, S_{max} or L on the GJW dispersion curves for a vortex sheet, depending on the Mach number.

For $M = 0.9$, as expected, tonal components sharply emerge at the Strouhal numbers mentioned above, obtained at stationary points S_{max}, corresponding to the saddle points S2 in references [19, 20], for this Mach number. The tones are due to GJW resonating in the jet potential core according to Towne et al. [19]. They are very similar for the four nozzle-lip thicknesses considered. Their amplitudes, in particular, do not differ by more than 1 dB. This can be explained by the fact that the upstream-propagating waves involved in the generation of these tones are mainly duct-like GJW with no amplitude in the jet shear layer, as discussed in Schmidt et al. [20] for instance. Thus, the nozzle lip plays no significant role in this case.

For the two other Mach numbers, in agreement with previous studies [19, 23, 52], the spectra are not dominated by tones. For the thinnest lip dlipx1, they are essentially broadband and contain peaks of limited level around the cut-off frequencies of the free-stream GJW, at points I for $M = 0.6$ and S_{max} or L for $M = 1.3$. As the nozzle lip increases, however, the peaks strengthen and additional peaks even emerge, by approximately 3 dB, around these frequencies. Therefore, contrary to the findings for $M = 0.9$, the presence of a thicker nozzle lip promotes the generation of tonal

7

components in the jet potential core for $M = 0.6$ and $M = 1.3$, through a mechanism involving upstream-propagating free-stream GJW reflecting at the nozzle lip in these two cases. For $M = 0.6$, in particular, one narrow peak appears near the frequency of the least-dispersed waves of the first axisymmetric GJW mode in figures 9(a). This shows that, provided that the nozzle lip is sufficiently thick, the least-dispersed GJW can contribute to the establishment of a feedback loop in free jets at $M = 0.6$, as was assumed by Tam and Ahuja [48] in a work on subsonic impinging jets thirty years ago.
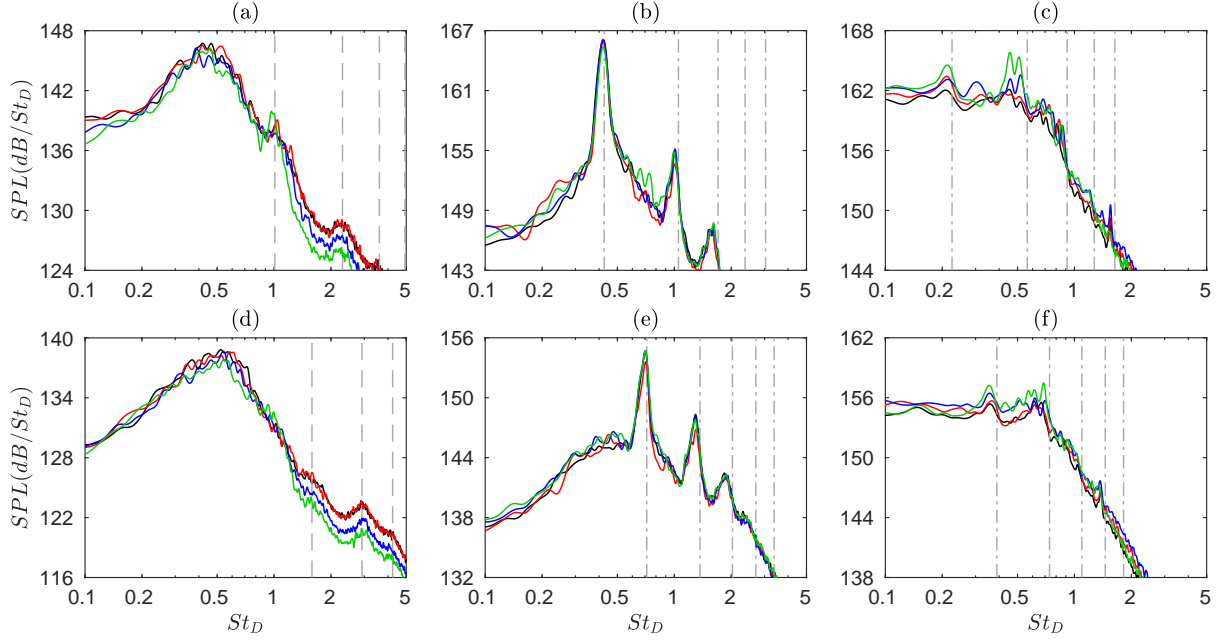
Fig. 7   Sound pressure levels obtained in the potential core between $z = 0$ and $z = z_c/2$ for (left) $M = 0.6$, (middle) $M = 0.9$ and (right) $M = 1.3$ at (a-c) $r = 0$ for $n_\theta = 0$ and (d-f) $r = 0.2r_0$ for $n_\theta = 1$: ——— dlipx1, ——— dlipx4, ——— dlipx16 and ——— dlipx64; cut-off Strouhal numbers of the first radial modes of the free-stream upstream-propagating GJW at points – – – I and – · – S_{max} or L on the GJW dispersion curves for a vortex sheet.

D. Pressure spectra near the nozzle exit

Finally, the presence of acoustic tones outside the jet flow near the nozzle is explored in the spectra of pressure fluctuations computed at $z = 0$ and $r = 2r_0$. The spectra are represented in figure 8 as a function of St_D. The contributions of the azimuthal modes $n_\theta = 0$, 1 and 2 to the spectra are depicted in figures 9(left) for $M = 0.6$, in figures 9(middle) for $M = 0.9$ and in figures 9(right) for $M = 1.3$. The spectra are those obtained for the nozzle-lip thicknesses dlipx1, dlipx16 and dlipx64, from top to bottom. The results for dlipx4 are not provided because they are very similar to those for dlipx1. The cut-off Strouhal numbers of the first two radial modes of the free-stream upstream-propagating GJW predicted by a vortex-sheet model are also indicated, in the same way as in the two previous sections.

In agreement with the data available in the literature for jets at similar Mach numbers [18, 22, 23, 26, 53], the near-nozzle spectra for $M = 0.9$ and $M = 1.3$ are dominated by intense tones in figures 8(b-c) and figures 9(middle-right), whereas the spectra for $M = 0.6$ are not but overall exhibit broadband peaks in figure 8(a) and figures 9(left). Not surprisingly, the main peaks and tones are associated with the first three azimuthal modes. In order to better quantify the variations of their characteristics with the nozzle-lip thickness, the Strouhal numbers of the two strongest peaks obtained for the axisymmetric mode in each case are plotted in figures 10 as a function of the lip thickness. The levels and full widths at half maximum of the peaks for the modes $n_\theta = 0$, 1 and 2 are also given in figures 11 and 12, respectively.

The peak frequencies in the spectra of figure 9 are located near the cut-off Strouhal numbers of the free-stream GJW in most cases, as observed in previous studies, and they do not vary significantly with the nozzle-lip thickness.

8
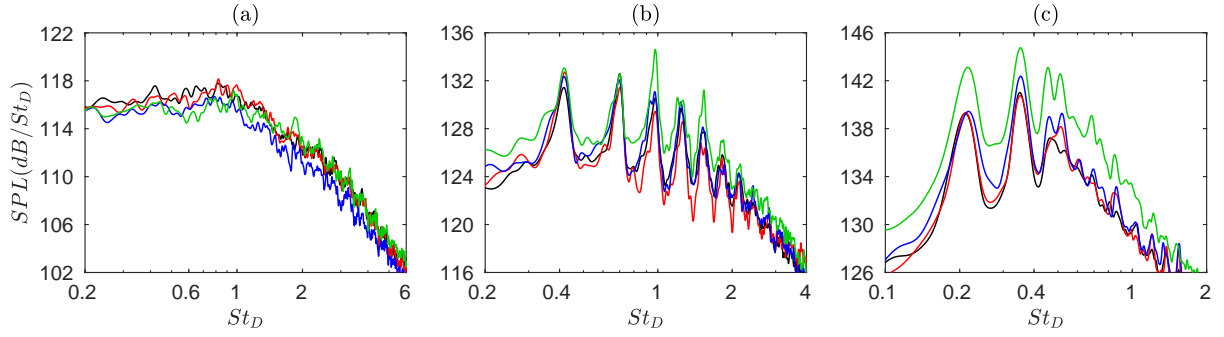
Fig. 8 **Sound pressure levels at $z = 0$ and $r = 2r_0$ for (a) $M = 0.6$, (b) $M = 0.9$ and (c) $M = 1.3$:** ——— **dlipx1,** ——— **dlipx4,** ——— **dlipx16 and** ——— **dlipx64.**
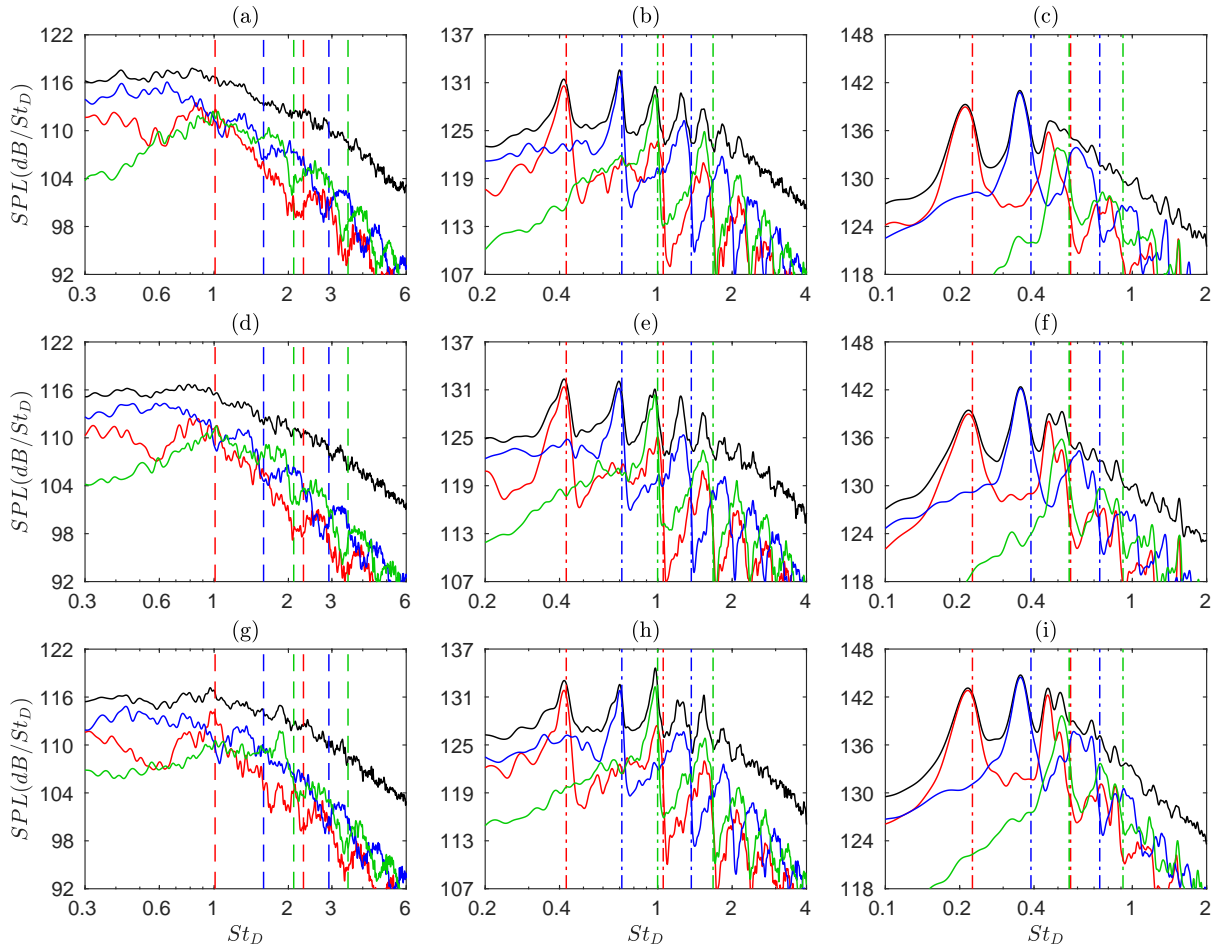

Fig. 9 **Sound pressure levels at $z = 0$ and $r = 2r_0$ for (left) $M = 0.6$, (middle) $M = 0.9$ and (right) $M = 1.3$ with (a-c) dlipx1, (d-f) dlipx16 and (g-i) dlipx64:** ——— **total,** ——— $n_\theta = 0$, ——— $n_\theta = 1$ **and** ——— $n_\theta = 2$; **cut-off Strouhal numbers of the first two radial modes of the free-stream upstream-propagating GJW at points (dashed lines) I and (dash-dotted lines) S_{max} or L on the GJW dispersion curves for a vortex sheet using the same colors as for the solid lines.**

9

These results are clearly illustrated in figure 10 representing the peak Strouhal numbers together with the allowable frequency ranges of the waves mentioned above for $n_\theta = 0$ (similar trends are obtained for the peak frequencies for $n_\theta = 1$ and 2, not shown for brevity).
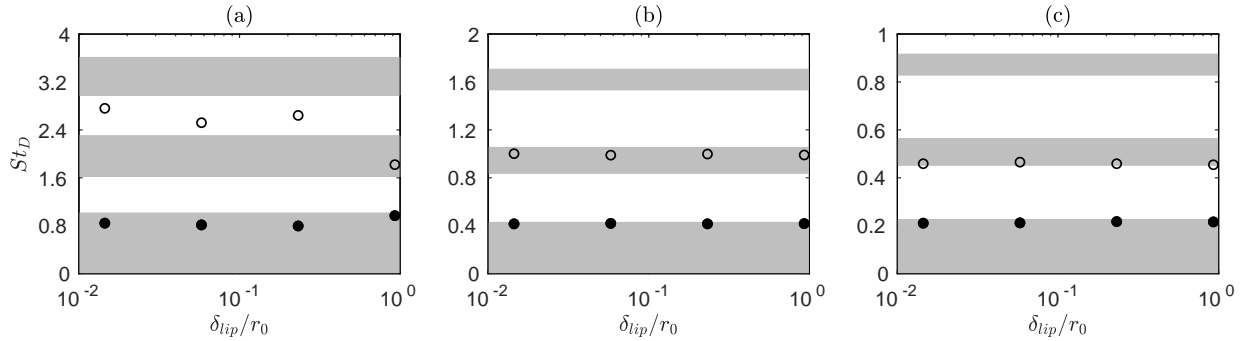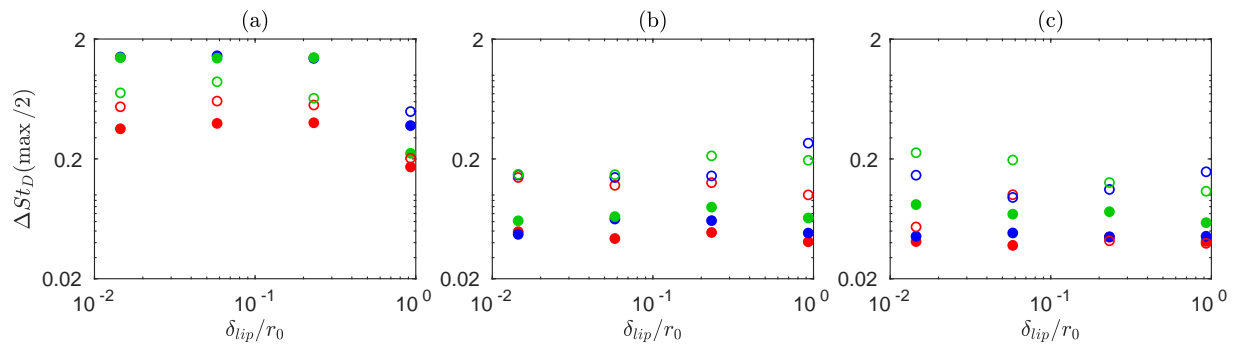

Fig. 10   Variations of the near-nozzle peak Strouhal numbers with δ_{lip}/r_0 for (a) $M = 0.6$, (b) $M = 0.9$ and (c) $M = 1.3$ for $n_\theta = 0$: ● dominant and ○ second strongest peaks; (grey) frequency ranges of the free-stream upstream-propagating GJW for a vortex sheet.

Regarding the peak prominence and levels, they visibly change with the lip thickness. However, the changes are quite weak between lipx1 and lipx16 with $\delta_{lip} \leq 0.23r_0$ and are more pronounced using dlipx64 with $\delta_{lip} = 0.93r_0$. They also depend on the Mach number. More precisely, as the nozzle-lip thickness increases, for $M = 0.9$ and $M = 1.3$, the levels of the near-nozzle tones rise in figures 11(b,c), whereas their widths remain essentially the same in figures 12(b,c). The gain is higher in the supersonic case than in the subsonic case, and reaches, at most, 6 dB and 3 dB, respectively. For $M = 0.6$, the broadband peaks appearing in the spectra for the three thinnest lips turn into 2 dB stronger, 2 to 4 times narrower peaks for the thickest lip, according to figures 11(a) and 12(a). This leads, for instance, to the small tonal components emerging around $St_D = 1$ for $n_\theta = 0$ and $St_D = 2$ for $n_\theta = 2$ in figure 9(g), near the frequencies of the least-dispersed GJW of the first radial modes also for $n_\theta = 0$ and 2.
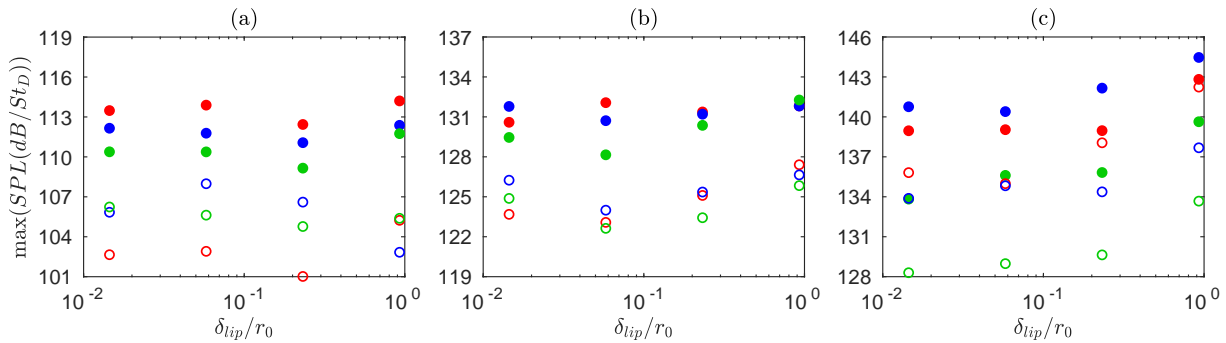
Fig. 11   Variations of near-nozzle peak levels with δ_{lip}/r_0 for (a) $M = 0.6$, (b) $M = 0.9$ and (c) $M = 1.3$: (filled circles) dominant and (open circles) second strongest peaks for (red) $n_\theta = 0$, (blue) $n_\theta = 1$ and (green) $n_\theta = 2$.

Therefore, for the present free jets, the use of the thickest nozzle lip results in stronger or additional near-nozzle tonal components at the three Mach numbers considered, even at the lowest one for which it was rather unexpected. Given their frequencies, these tones are most probably all related to upstream-propagating free-stream GJW reflecting back at the nozzle lip, close to the frequencies of the least-dispersed GJW for $M = 0.6$ and to those of the stationary GJW for $M = 0.9$ and 1.3. Based on the results in previous section, it then appears that the tonal components in the potential core and those outside the flow near the nozzle are generated by phenomena involving upstream-propagating GJW of the same kind for $M = 0.6$ and 1.3 (free-stream GJW) but of different kinds for $M = 0.9$ (duct-like GJW inside the potential core and free-stream GJW outside).

Fig. 12 Variations of near-nozzle peak widths with δ_{lip}/r_0 for (a) $M = 0.6$, (b) $M = 0.9$ and (c) $M = 1.3$: (filled circles) dominant and (open circles) second strongest peaks for (red) $n_\theta = 0$, (blue) $n_\theta = 1$ and (green) $n_\theta = 2$.

IV. Conclusion

In this paper, the influence of the nozzle-lip thickness on the acoustic tones emerging in the pressure spectra in the potential core and near the nozzle of free jets has been investigated using well-resolved LES for jet Mach numbers $M = 0.6$, 0.9 and 1.3 and nozzle-lip thicknesses varying between $0.01r_0$ and $0.9r_0$. With one exception, the use of a thicker lip leads to stronger tonal components at the cut-off frequencies of the upstream-propagating free-stream GJW modes, obtained at the frequencies of the least-dispersed GJW for $M = 0.6$ and of the stationary GJW for $M = 0.9$ and 1.3. This strengthening can be attributed to a greater efficiency of the receptivity process near the lip as the the upstream-propagating waves are reflected back over a larger surface. These results show that the upstream-propagating free-stream GJW play a key role in the establishment of feedback loops in free jets, producing tones both inside and outside the jets, even at $M = 0.6$. The exception is for the tones inside the potential core for $M = 0.9$, whose levels are nearly insensitive to the change in the lip thickness, and which are, consequently, most likely generated by a resonance mechanism involving upstream-propagating duct-like GJW.

Further analyzes could be made to complement this work. In particular, the efficiency of the receptivity process could be assessed by evaluating how much upstream-propagating acoustic waves are scattered back into shear-layer Kelvin-Helmholtz instability waves for the four nozzle lips considered. Obviously, it will be necessary to better identify and describe the feedback loops and resonance mechanisms occurring in the different cases. With this aim, several techniques, based on wavenumber-frequency Fourier transforms and the Proper Decomposition Method (POD) for instance, could be useful. It would also be interesting to search for the presence of standing-wave patterns in the r.m.s. jet near pressure fields at the tone frequencies, because such patterns can provide information on the upstream-propagating waves and the downstream-propagating waves involved in the feedback loops.

Acknowledgments

References

[1] Raman, G., "Supersonic jet screech: half-century from Powell to the present," *J. Sound Vib.*, Vol. 225, No. 3, 1999, pp. 543–571. https://doi.org/10.1006/jsvi.1999.2181.

[2] Edgington-Mitchell, D., "Aeroacoustic resonance and self-excitation in screeching and impinging supersonic jets - A review," *Int. J. Aeroacoust.*, Vol. 18, No. 2-3, 2019, pp. 118–188. https://doi.org/10.1177/1475472X19834521.

[3] Karami, S., Stegeman, P. C., Ooi, A., Theofilis, V., and Soria, J., "Receptivity characteristics of under-expanded supersonic impinging jets," *J. Fluid Mech.*, Vol. 889, No. A27, 2020. https://doi.org/10.1017/jfm.2020.63.

[4] Mancinelli, M., Jaunet, V., Jordan, P., and Towne, A., "A complex-valued resonance model for axisymmetric screech tones in supersonic jets," *J. Fluid Mech.*, Vol. 928, 2021, p. A32. https://doi.org/10.1017/jfm.2021.848.

[5] Weightman, J. L., Amili, O., Honnery, D., Edgington-Mitchell, D., and Soria, J., "Nozzle external geometry as a boundary condition for the azimuthal mode selection in an impinging underexpanded jet," *J. Fluid Mech.*, Vol. 862, 2019, pp. 421–448. https://doi.org/10.1017/jfm.2018.957.

[6] Karami, S., and Soria, J., "Influence of nozzle external geometry on wavepackets in under-expanded supersonic impinging jets," *J. Fluid Mech.*, Vol. 929, No. A20, 2021. https://doi.org/10.1017/jfm.2021.822.

[7] Powell, A., "The reduction of choked jet noise," *Proc. Phys. Soc. B*, Vol. 67, No. 4, 1954, pp. 313–327. https://doi.org/10.1088/0370-1301/67/4/306.

[8] Norum, T. D., "Screech suppression in supersonic jets," *AIAA J.*, Vol. 21, No. 2, 1983, pp. 235–240. https://doi.org/10.2514/3.8059.

[9] Ponton, M. K., and Seiner, J. M., "The effects of nozzle exit lip thickness on plume resonance," *J. Sound Vib.*, Vol. 154, No. 3, 1992, pp. 531–549. https://doi.org/10.1016/0022-460X(92)90784-U.

[10] Raman, G., "Cessation of screech in underexpanded jets," *J. Fluid Mech.*, Vol. 336, 1997, pp. 69–90. https://doi.org/10.1017/S002211209600451X.

[11] Shen, H., and Tam, C. K. W., "Effects of jet temperature and nozzle-lip thickness on screech tones," *AIAA J.*, Vol. 38, No. 5, 2000, pp. 762–767. https://doi.org/10.2514/2.1055.

[12] Olsen, W. A., Gutierrez, O., and Dorsch, R. G., "The effect of nozzle inlet shape, lip thickness, and exit shape and size on subsonic jet noise," Tech. Rep. 73-187, AIAA Paper, 1973. https://doi.org/10.2514/6.1973-187.

[13] Fontaine, R. A., Elliott, G. S., Austin, J. M., and Freund, J. B., "Very near-nozzle shear-layer turbulence and jet noise," *J. Fluid Mech.*, Vol. 770, 2015, pp. 27–51. https://doi.org/10.1017/jfm.2015.119.

[14] Zaman, K. B. M. Q., "Effect of initial condition on subsonic jet noise from two rectangular nozzles," Tech. Rep. 2012-2160, AIAA Paper, 2012. https://doi.org/10.2514/6.2012-2160.

[15] Zaman, K. B. M. Q., "Effect of initial boundary-layer state on subsonic jet noise," *AIAA J.*, Vol. 50, No. 8, 2012, pp. 1784–1795. https://doi.org/10.2514/1.J051712.

[16] Laufer, J., and Monkewitz, P., "On turbulent jet flows: a new perspective," Tech. Rep. 80-0962, AIAA Paper, 1980. https://doi.org/10.2514/6.1980-962.

[17] Ho, C.-M., and Huang, L.-S., "Subharmonics and vortex merging in mixing layers," *J. Fluid Mech.*, Vol. 119, 1982, pp. 443–473. https://doi.org/10.1017/S0022112082001438.

[18] Suzuki, T., and Colonius, T., "Instability waves in a subsonic round jet detected using a near-field phased microphone array," *J. Fluid Mech.*, Vol. 565, 2006, pp. 197–226. https://doi.org/10.1017/S0022112006001613.

[19] Towne, A., Cavalieri, A. V. G., Jordan, P., Colonius, T., Schmidt, O., Jaunet, V., and Brès, G. A., "Acoustic resonance in the potential core of subsonic jets," *J. Fluid Mech.*, Vol. 825, 2017, pp. 1113–1152. https://doi.org/10.1017/jfm.2017.346.

[20] Schmidt, O., Towne, A., Colonius, T., Cavalieri, A. V. G., Jordan, P., and Brès, G. A., "Wavepackets and trapped acoustic modes in a turbulent jet: Coherent structure eduction and global stability," *J. Fluid Mech.*, Vol. 825, 2017, pp. 1153–1181. https://doi.org/10.1017/jfm.2017.407.

[21] Brès, G. A., Jordan, P., Jaunet, V., Le Rallic, M., Cavalieri, A. V. G., Towne, A., Lele, S. K., Colonius, T., and Schmidt, O. T., "Importance of the nozzle-exit boundary-layer state in subsonic turbulent jets," *J. Fluid Mech.*, Vol. 851, 2018, pp. 83–124. https://doi.org/10.1017/jfm.2018.476.

[22] Zaman, K. B. M. Q., Fagan, A. F., and Upadhyay, P., "Pressure fluctuations due to 'trapped waves' in the initial region of compressible jets," *J. Fluid Mech.*, Vol. 931, 2022, p. A30. https://doi.org/10.1017/jfm.2021.954.

[23] Bogey, C., "Acoustic tones in the near-nozzle region of jets: characteristics and variations between Mach numbers 0.5 and 2," *J. Fluid Mech.*, Vol. 921, 2021, p. A3. https://doi.org/10.1017/jfm.2021.426.

[24] Bogey, C., "Tones in the acoustic far field of jets in the upstream direction," *AIAA J.*, Vol. 60, No. 4, 2022, pp. 2397–2406. https://doi.org/10.2514/1.J061013.

[25] Tam, C. K. W., and Hu, F. Q., "On the three families of instability waves of high-speed jets," *J. Fluid Mech.*, Vol. 201, 1989, pp. 447–483. https://doi.org/10.1017/S002211208900100X.

[26] Bogey, C., "Interactions between upstream-propagating guided jet waves and shear-layer instability waves near the nozzle of subsonic and nearly ideally expanded supersonic free jets with laminar boundary layers," *J. Fluid Mech.*, Vol. 949, 2022, p. A41. https://doi.org/10.1017/jfm.2022.776.

[27] Bogey, C., and Bailly, C., "Influence of nozzle-exit boundary-layer conditions on the flow and acoustic fields of initially laminar jets," *J. Fluid Mech.*, Vol. 663, 2010, pp. 507–539. https://doi.org/10.1017/S0022112010003605.

[28] Bogey, C., Marsden, O., and Bailly, C., "Influence of initial turbulence level on the flow and sound fields of a subsonic jet at a diameter-based Reynolds number of 10^5," *J. Fluid Mech.*, Vol. 701, 2012, pp. 352–385. https://doi.org/10.1017/jfm.2012.162.

[29] Bogey, C., Marsden, O., and Bailly, C., "Large-Eddy Simulation of the flow and acoustic fields of a Reynolds number 10^5 subsonic jet with tripped exit boundary layers," *Phys. Fluids*, Vol. 23, No. 3, 2011, p. 035104. https://doi.org/10.1063/1.3555634.

[30] Bogey, C., "Grid sensitivity of flow field and noise of high-Reynolds-number jets computed by large-eddy simulation," *Int. J. Aeroacoust.*, Vol. 17, No. 4-5, 2018, pp. 399–424. https://doi.org/10.1177/1475472X18778287.

[31] Bogey, C., and Sabatini, R., "Effects of nozzle-exit boundary-layer profile on the initial shear-layer instability, flow field and noise of subsonic jets," *J. Fluid Mech.*, Vol. 876, 2019, pp. 288–325. https://doi.org/10.1017/jfm.2019.546.

[32] Zaman, K. B. M. Q., "Effect of initial condition on subsonic jet noise," *AIAA J.*, Vol. 23, No. 9, 1985, pp. 1370–1373. https://doi.org/10.2514/3.9094.

[33] Mohseni, K., and Colonius, T., "Numerical treatment of polar coordinate singularities," *J. Comput. Phys.*, Vol. 157, No. 2, 2000, pp. 787–795. https://doi.org/10.1006/jcph.1999.6382.

[34] Bogey, C., de Cacqueray, N., and Bailly, C., "Finite differences for coarse azimuthal discretization and for reduction of effective resolution near origin of cylindrical flow equations," *J. Comput. Phys.*, Vol. 230, No. 4, 2011, pp. 1134–1146. https://doi.org/10.1016/j.jcp.2010.10.031.

[35] Bogey, C., and Bailly, C., "A family of low dispersive and low dissipative explicit schemes for flow and noise computations," *J. Comput. Phys.*, Vol. 194, No. 1, 2004, pp. 194–214. https://doi.org/10.1016/j.jcp.2003.09.003.

[36] Bogey, C., de Cacqueray, N., and Bailly, C., "A shock-capturing methodology based on adaptive spatial filtering for high-order non-linear computations," *J. Comput. Phys.*, Vol. 228, No. 5, 2009, pp. 1447–1465. https://doi.org/10.1016/j.jcp.2008.10.042.

[37] Berland, J., Bogey, C., Marsden, O., and Bailly, C., "High-order, low dispersive and low dissipative explicit schemes for multiple-scale and boundary problems," *J. Comput. Phys.*, Vol. 224, No. 2, 2007, pp. 637–662. https://doi.org/10.1016/j.jcp.2006.10.017.

[38] Tam, C. K. W., and Dong, Z., "Radiation and outflow boundary conditions for direct computation of acoustic and flow disturbances in a nonuniform mean flow," *J. Comput. Acous.*, Vol. 4, No. 2, 1996, pp. 175–201. https://doi.org/10.1142/S0218396X96000040.

[39] Bogey, C., and Bailly, C., "Large Eddy Simulations of transitional round jets: influence of the Reynolds number on flow development and energy dissipation," *Phys. Fluids*, Vol. 18, No. 6, 2006, p. 065101. https://doi.org/10.1063/1.2204060.

[40] Fauconnier, D., Bogey, C., and Dick, E., "On the performance of relaxation filtering for large-eddy simulation." *J. Turbulence*, Vol. 14, No. 1, 2013, pp. 22–49. https://doi.org/10.1080/14685248.2012.740567.

[41] Kremer, F., and Bogey, C., "Large-eddy simulation of turbulent channel flow using relaxation filtering: Resolution requirement and Reynolds number effects," *Comput. Fluids*, Vol. 116, 2015, pp. 17–28. https://doi.org/10.1016/j.compfluid.2015.03.026.

[42] Bogey, C., "A database of flow and near pressure field signals obtained for subsonic and nearly ideally expanded supersonic free jets using large-eddy simulations," https://hal.archives-ouvertes.fr/hal-03626787, 2022.

[43] Winant, C., and Browand, F., "Vortex pairing : the mechanism of turbulent mixing-layer growth at moderate Reynolds number," *J. Fluid Mech.*, Vol. 63, No. 2, 1974, pp. 237–255. https://doi.org/10.1017/S0022112074001121.

[44] Michalke, A., "Survey on jet instability theory," *Prog. Aerosp. Sci.*, Vol. 21, 1984, pp. 159–199. https://doi.org/10.1016/0376-0421(84)90005-8.

[45] Morris, P. J., "The instability of high speed jets," *Int. J. Aeroacoust.*, Vol. 9, No. 1-2, 2010, pp. 1–50. https://doi.org/10.1260/1475-472X.9.1-2.1.

[46] Arndt, R. E. A., Long, D. F., and Glauser, M. N., "The proper orthogonal decomposition of pressure fluctuations surrounding a turbulent jet," *J. Fluid Mech.*, Vol. 340, 1997, pp. 1–33. https://doi.org/10.1017/S0022112097005089.

[47] Bogey, C., "Generation of excess noise by jets with highly disturbed laminar boundary-layer profiles," *AIAA J.*, Vol. 59, No. 2, 2021, pp. 569–579. https://doi.org/10.2514/1.J059610.

[48] Tam, C. K. W., and Ahuja, K. K., "Theoretical model of discrete tone generation by impinging jets," *J. Fluid Mech.*, Vol. 214, 1990, pp. 67–87. https://doi.org/10.1017/S0022112090000052.

[49] Bradshaw, P., "The effect of initial conditions on the development of a free shear layer," *J. Fluid Mech.*, Vol. 26, No. 2, 1966, pp. 225–236. https://doi.org/10.1017/S0022112066001204.

[50] Browand, F. K., and Latigo, B. O., "Growth of the two-dimensional mixing layer from a turbulent and nonturbulent boundary layer," *Phys. Fluids*, Vol. 22, No. 6, 1979, pp. 1011–1019. https://doi.org/10.1063/1.862705.

[51] Zaman, K. B. M. Q., and Hussain, A. K. M. F., "Vortex pairing in a circular jet under controlled excitation. Part 1. General jet response." *J. Fluid Mech.*, Vol. 101, No. 3, 1980, pp. 449–491. https://doi.org/10.1017/S0022112080001760.

[52] Towne, A., Schmidt, O. T., and Brès, G. A., "An investigation of the Mach number dependence of trapped acoustic waves in turbulent jets," Tech. Rep. 2019-2546, AIAA Paper, 2019. https://doi.org/10.2514/6.2019-2546.

[53] Jaunet, V., Jordan, P., Cavalieri, A. V. G., Towne, A., Colonius, T., Schmidt, O., and Brès, G. A., "Tonal dynamics and sound in free and installed turbulent jets," Tech. Rep. 2016-3016, AIAA Paper, 2016. https://doi.org/10.2514/6.2016-3016.